



Contents lists available at ScienceDirect

Arabian Journal of Chemistry

journal homepage: www.sciencedirect.com



Original article

# Fe<sub>3</sub>O<sub>4</sub>-chitosan immobilized Cu(II) Schiff base catalyst for the microwave-assisted amination of aryl halides in water

Kamrul Hasan<sup>a,\*</sup>, Reshma G Joseph<sup>a</sup>, Ihsan A. Shehadi<sup>a</sup>, Shashikant P. Patole<sup>b</sup><sup>a</sup> Department of Chemistry, Pure and Applied Chemistry Group, College of Sciences, University of Sharjah, P.O. Box 27272, Sharjah, United Arab Emirates<sup>b</sup> Department of Physics, Khalifa University of Science and Technology, P.O. Box 127788, Abu Dhabi, United Arab Emirates

## ARTICLE INFO

## Article history:

Received 29 March 2023

Accepted 27 September 2023

Available online 4 October 2023

## Keywords:

Fe<sub>3</sub>O<sub>4</sub>-chitosan

Schiff base

Copper

C-N coupling

Amination

## ABSTRACT

This work represents the synthesis, characterization, and application of a magnetically separable (Fe<sub>3</sub>O<sub>4</sub>@CS@AF@Cu) catalyst for the C-N coupling reaction towards arylation of amines. The catalyst is synthesized by modifying the surface of Fe<sub>3</sub>O<sub>4</sub>-chitosan with acetyl-2-furan (AF) via the formation of Schiff base and then, generating a Cu(II) complex on the functionalized surface. State-of-art characterization techniques such as Fourier-transform infrared spectroscopy (FTIR), thermogravimetric analysis (TGA), field-emission scanning electron microscopy (FE-SEM), energy dispersive X-ray spectrometry (EDX), transmission electron microscopy (TEM), X-ray diffractometer (XRD), x-ray photoelectron spectroscopy (XPS) and inductively coupled plasma-optical emission (ICP-OES) spectrometry have been used to verify the structure of the catalyst. Under microwave irradiation, the Ullmann C-N coupling reactions using various aryl halides and amines demonstrate exceptional catalytic performance with a minimal catalyst loading of 0.63 mol% of Cu. Furthermore, the catalyst has been recycled 5 times with 96% efficiency for the amination of 1-bromo-4-nitrobenzene with piperidine under the investigated conditions. Overall, this study provides a practical approach to the synthesis of an effective heterogeneous catalyst for the C-N coupling reaction, which can be used in pharmaceuticals, bulk, and fine chemical industries. © 2023 The Author(s). Published by Elsevier B.V. on behalf of King Saud University. This is an open access article under the CC BY-NC-ND license (<http://creativecommons.org/licenses/by-nc-nd/4.0/>).

## 1. Introduction

N-arylation of amine *via* the formation of aryl amine is a promising area of research due to its application as building blocks for plenty of pharmaceutical drugs, dyes, pigments, and polymers (Aubin et al., 2010, Yadav et al., 2019). One of the common methods for converting aryl halides into amines involves the use of ammonia as a nucleophile at elevated temperatures and pressure (Lang et al., 2001). Ammonia is a relatively inexpensive reagent that is widely used in organic synthesis. However, in certain synthesis routes, ammonia may lead to the formation of complicated side products due to the highly unstable nature of aryl intermediates. In 1990 s, a breakthrough is achieved by Buchwald (Wagaw and Buchwald 1996) and Hartwig (Hartwig et al., 1999) *via*

palladium-catalysed amination of aryl halides with ammonia through C-N coupling. However, this catalytic system suffers from drawbacks as, air sensitivity, reaction toxicity, and high cost of palladium which limits their application for the large-scale production of arylamines in the industrial fields (Zhang et al., 2014, Dorel et al., 2019). Later, copper catalysed Ullmann type reaction has emerged as a promising alternative to the expensive and toxic palladium-based methods for the C-N coupling reactions (Hazari et al., 2017, Lo et al., 2018, Gómez-Orellana et al., 2021). Since then, various classes of ligand have been developed and explored the homogenous Cu-complexes for promoting the C-N coupling reactions for versatile organic syntheses. However, these homogenous catalytic systems have certain disadvantages such as a complicated and multi-step ligand synthesis, un-recyclability of catalysts, and potential toxicity of solvents (DMF, DMSO, dioxane etc) employed as reaction media (Hasan and Zysman-Colman 2013, Ge et al., 2018, Liu et al., 2018, Ge et al., 2019). In addition, catalysts with homogeneous behaviour have many advantages like excellent activity, chemo- and regioselectivity, high product yield, and high turnover number. Problems associated with time-consuming separation, recovery, and recyclability of the catalyst restrict their performance in industrial applications (Pelletier and Basset 2016, Xie et al., 2018). Therefore, further improvement in the fabrication of

\* Corresponding author.

E-mail address: [khasan@sharjah.ac.ae](mailto:khasan@sharjah.ac.ae) (K. Hasan).

Peer review under responsibility of King Saud University.



Production and hosting by Elsevier

environmentally benign heterogeneous catalyst along with green alternative solvents for the Ullmann type C–N coupling reactions are needed to be flourished.

Recently, a substantial amount of research has been focusing on the development of sustainable, cost-effective, and environmentally-friendly heterogeneous catalysts in the industrial field (Baek et al., 2018). Noticeably, the heterogeneous catalysts have very impressive characteristics like easy separation from the reaction mixture, recyclability, reusability, and much lower leaching (Khaleel et al., 2010, Khaleel et al., 2011). However, the activity and selectivity for the heterogeneous catalysts are usually less compared to homogeneous ones (Moulijn et al., 1993, Panigrahi et al., 2007). Therefore, bringing homogenous catalyst's high activity and selectivity in the heterogenous catalyst's support known as "Tethered catalyst" is an attractive method for the design of new catalysts. Among the available heterogeneous catalyst supports, the magnetic nanoparticles (MNPs) have achieved ample attention because of their low toxicity, biocompatibility, exemplary chemical and thermal stability, and high surface area to volume ratio (Zhang et al., 2016, Terrasson and Guenin 2018, Cai et al., 2019). Most of all, the major advantage of using MNPs is the ease of recovery using an external magnet. Fe<sub>3</sub>O<sub>4</sub> is one of the most promising MNPs due to its simple preparation from low-cost precursors, high surface area, low toxicity, fantastic reusability, and biocompatibility (Moradi et al., 2020). However, bare Fe<sub>3</sub>O<sub>4</sub> is vulnerable to oxidation and self-aggregation (Tajyani and Babaei, 2018). Hence, it is essentially required to protect the surface of Fe<sub>3</sub>O<sub>4</sub> by a suitable coating agent through surface functionalization. Among the various coating agents, mesoporous silica, cellulose, and chitosan are very attractive for surface functionalization of Fe<sub>3</sub>O<sub>4</sub> (Liu et al., 2012, Sharma et al., 2014, Bromho et al., 2018, Sun et al., 2019). Up to date, varieties of heterogeneous copper catalysts have been developed by the decoration and coordination of copper on different support materials. These include carbon (Zhang et al., 2013), alumina (Reddy et al., 2015), zeolites (Raiza et al., 2019), polymers (Islam et al., 2012, Yi et al., 2018), and magnetic materials (Chouhan et al., 2007, Panda et al., 2011), all of which have demonstrated catalytic performance in facilitating the Ullmann C–N coupling reactions. However, our research focuses on the development of heterogenous catalyst through modification of environmentally benign and bio-renewable resourced based Fe<sub>3</sub>O<sub>4</sub>-chitosan surface.

Chitosan (CS), poly[(1–4)-linked-2-amino-2-deoxy-d'glucose], is the most abundant natural amino polysaccharide, that is produced by the deacetylation of chitin (Rana et al., 2009, Ulu et al., 2020). Chitosan plays an important role as a protective layer to Fe<sub>3</sub>O<sub>4</sub> due to their excellent properties like non-toxicity, hydrophilicity, biocompatibility, and biodegradability (Lei et al., 2009). The presence of free, active amino groups and hydroxyl groups on the surface of chitosan allow many chemical modifications like carboxylation (Xu et al., 2021), imination (Iftime et al., 2017), acylation (Sashiwa et al., 2002), sulfation (Jayakumar et al., 2007), enzymatic substitution (Poshina et al., 2018), nitration (Kim et al., 2016), metal chelation (Monier et al., 2010), cyanoethylation (Diab et al., 2012) and phosphorylation (Wu et al., 2019). The Schiff base condensation of the chitosan NH<sub>2</sub> groups with carbonyl group through the formation of imine functional groups is one of the most important modifications of chitosan (Duan et al., 2009, Mohammadikish and Hashemi 2019, Shahraki et al., 2019).

In the development of green and sustainable catalyst, our research group is focusing Fe<sub>3</sub>O<sub>4</sub> based heterogeneous catalysts for significant organic synthesis, including nitroarene reduction (Hasan et al., 2019), C–C cross-coupling (Hasan 2020, Hasan et al., 2022), oxidative amination (Hasan et al., 2022), A<sup>3</sup> coupling (Hasan et al., 2023), and ester synthesis (Ahmad et al., 2021). In this work, we functionalize Fe<sub>3</sub>O<sub>4</sub>-chitosan surface with acetyl-2-

furan via the formation of Schiff base ligand following the generation of Cu(II) complex. To our delight, the fabricated magnetic chitosan immobilized Cu(II) Schiff base complex Fe<sub>3</sub>O<sub>4</sub>@CS@AF@Cu exhibits excellent catalytic performance for the amination of aryl halides via the Ullmann C–N coupling reaction under microwave irradiation. Detailed synthetic route of the catalyst material Fe<sub>3</sub>O<sub>4</sub>@CS@AF@Cu represented in the Scheme 1. Moreover, the prepared catalyst exhibits exceptional durability in environmentally benign solvent water and can be reused up to five times without any significant loss of its catalytic efficiency.

## 2. Materials and methods

### 2.1. Synthesis of magnetic Fe<sub>3</sub>O<sub>4</sub> and coating with chitosan (Fe<sub>3</sub>O<sub>4</sub>@CS)

The synthesis of magnetic Fe<sub>3</sub>O<sub>4</sub> and coating with chitosan are conducted by adapting previously published methods (Hasan et al., 2019).

### 2.2. Synthesis of Fe<sub>3</sub>O<sub>4</sub>@CS@AF

The procedure for generating a Schiff base onto the Fe<sub>3</sub>O<sub>4</sub>-CS surface, which was carried out using a previously reported method (Hasan et al., 2023). The process involved adding 1.5 g of Fe<sub>3</sub>O<sub>4</sub>@CS to a 250 mL round bottom flask containing 25 mL of EtOH, which was then set with a reflux condenser. Next, 1.38 g (12.5 mmol) of acetyl-2-furan was added to the reaction mixture and was reflux at 78 °C for 48 h under an argon atmosphere. Upon completion of the reaction, the product Fe<sub>3</sub>O<sub>4</sub>@CS@AF was separated using an external magnet and washed two times with ethanol (2 × 25.0 mL) to remove any unreacted acetyl-2-furan. Then, the final product was dried in vacuum at 60 °C for 8 h.

### 2.3. Synthesis of Fe<sub>3</sub>O<sub>4</sub>@CS@AF@Cu

A 1.20 g of Fe<sub>3</sub>O<sub>4</sub>@CS@AF and 0.27 g of Cu(II)Cl<sub>2</sub>·H<sub>2</sub>O were added into 75 mL of EtOH, and the resulting slurry was reflux at 80 °C for 48 h. The progress of the reaction was monitored by the disappearance of colour in the Cu(II)Cl<sub>2</sub>·H<sub>2</sub>O solution. After the reaction was completed, the final product was separated from the reaction mixture using an external magnet. The resulting brown solid catalyst Fe<sub>3</sub>O<sub>4</sub>@CS@AF@Cu was then washed with EtOH followed by acetone and dried in vacuum for 6 h at 70 °C.

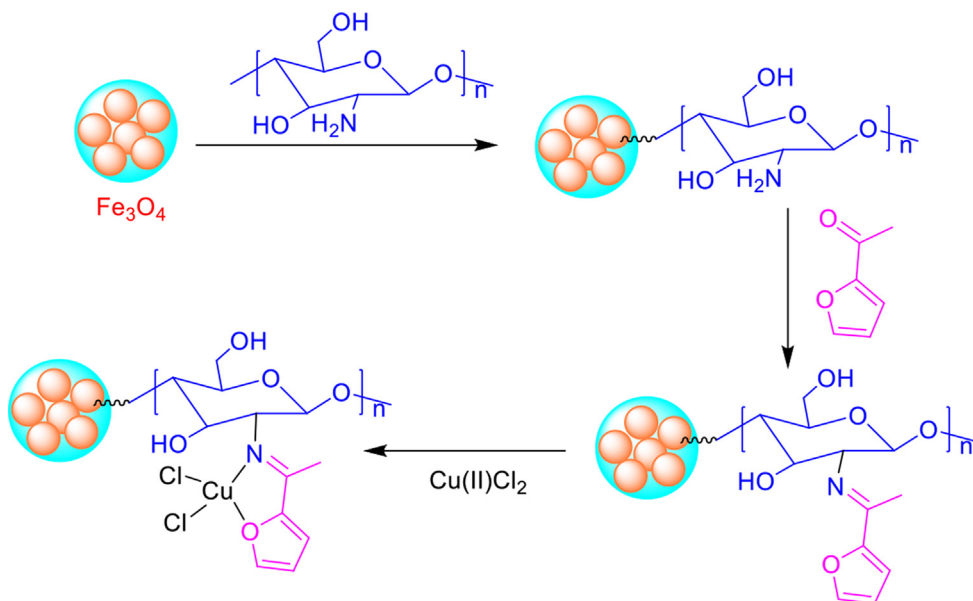
### 2.4. General procedure for the amination of aryl halides

A 1.0 mmol of aryl halide, 1.1 mmol of amine and 2.0 mmol of K<sub>2</sub>CO<sub>3</sub> were added into a 10 mL microwave vial. Afterward, the reaction vessel was filled with 5 mL of H<sub>2</sub>O and 5.0 mg of catalyst, Fe<sub>3</sub>O<sub>4</sub>@CS@AF@Cu (0.63 mol% Cu) and placed in the cavity of a CEM Discover-focused microwave synthesis system. Subsequently, the reaction mixture was heated to 100 °C for an hour with 100 Psi and 100 Watts. After the reaction was completed, the product was isolated by performing liquid-liquid extraction with ethyl acetate three times (3 × 10 mL) using a separatory funnel. The combined organic phases were dried over Na<sub>2</sub>SO<sub>4</sub>. Then, the solvent was removed by rotatory evaporator and the products were analysed and verified via GC–MS and <sup>1</sup>H NMR analysis.

## 3. Results and discussion

### 3.1. Characterizations of the catalyst

The stepwise functionalization of the magnetite Fe<sub>3</sub>O<sub>4</sub> is confirmed by the FTIR spectra that is shown in Fig. 1. In the FTIR spec-



**Scheme 1.** Preparation route of the catalyst  $\text{Fe}_3\text{O}_4@CS@AF@Cu$ .

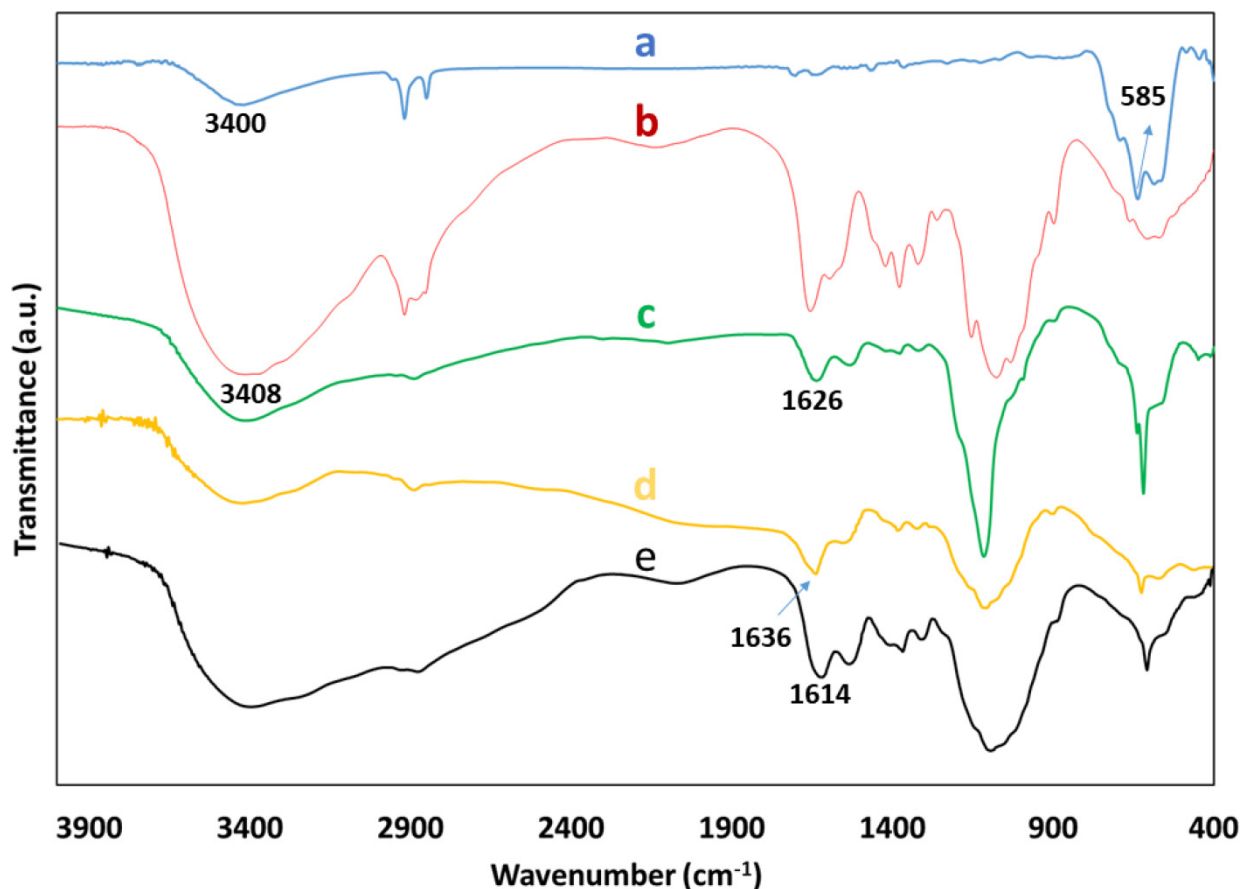


**Fig. 1.** FTIR spectra of  $\text{Fe}_3\text{O}_4$  (a), CS (b),  $\text{Fe}_3\text{O}_4@CS$  (c),  $\text{Fe}_3\text{O}_4@CS@AF$  (d), and  $\text{Fe}_3\text{O}_4@CS@AF@Cu$  (e).

trum of  $\text{Fe}_3\text{O}_4$  (Fig. 1, a), the presence of Fe-O stretching vibration is indicated by a pronounced absorption peak that is observed at  $585\text{ cm}^{-1}$ , while the -OH stretching vibration on the surface of  $\text{Fe}_3\text{O}_4$  is confirmed by a wide band at  $3400\text{ cm}^{-1}$ . The FTIR spectrum of CS (Fig. 1, b) shows broad band that is observed at  $3408\text{ cm}^{-1}$  that can be attributed to the overlapping stretching vibrations of both the -OH and -NH<sub>2</sub> groups in the CS moiety.

The successful coating of  $\text{Fe}_3\text{O}_4$  with CS in the  $\text{Fe}_3\text{O}_4@CS$  composite is confirmed by the stretching vibration of N-H at  $1626\text{ cm}^{-1}$  (Fig. 1, c). The formation of furan-imine (C = N) Schiff base ligand is confirmed by shifting of N-H stretching from  $1626$  to  $1636\text{ cm}^{-1}$  while  $\text{Fe}_3\text{O}_4@CS$  is treated with acetyl-2-furan under experimental conditions (Fig. 1, d). Finally, FTIR spectrum of the catalyst  $\text{Fe}_3\text{O}_4@CS@AF@Cu$  (Fig. 1, e) exhibits the generation of a

Schiff base complex of Cu(II) on the functionalized surface of Fe<sub>3</sub>O<sub>4</sub>-chitosan. Especially, C = N stretching band of the Schiff base is hypsochromically shifted by 22 cm<sup>-1</sup> while Cu(II) ion coordinated with N- and O- bonding atoms of the ligand in the Fe<sub>3</sub>O<sub>4</sub>@CS@AF@Cu materials.

Fig. 2 illustrates the TGA plots of Fe<sub>3</sub>O<sub>4</sub> (a), CS (b), Fe<sub>3</sub>O<sub>4</sub>@CS (c), Fe<sub>3</sub>O<sub>4</sub>@CS@AF (d), and Fe<sub>3</sub>O<sub>4</sub>@CS@AF@Cu (e) respectively. TGA plots reveal the thermal stability and nature of the components present in the composite materials which either contain solvent, moisture content, organic or inorganic moieties. For bare Fe<sub>3</sub>O<sub>4</sub>, the TGA curve shows that weight loss over the temperature range from 30 °C to 800 °C is only 4%. This might be due to the loss of moisture content in the sample of Fe<sub>3</sub>O<sub>4</sub>. However, all the TGA curves except Fe<sub>3</sub>O<sub>4</sub> (Fig. 2, a) exhibit pseudo two-stage decomposition with the increase of temperature. The first step of the thermal decomposition corresponds to the removal of moisture or remaining solvent content from the nanocomposites, and the next step is for the main mass loss which involves the removal of organic moieties from the chitosan and grafted Schiff base moiety from the materials.

The composites (Fig. 2, b-e) lose 10-15% of their weight within 200 °C mainly for the remaining solvent and moisture content and then onwards weight loss varies based on their organic and inorganic content ratio. TGA curve (Fig. 2, d) clearly shows that grafting of Schiff base on the magnetic-chitosan surface due to its higher weight loss that as compared to Fe<sub>3</sub>O<sub>4</sub>@CS (Fig. 2, c). Finally, the target catalyst material Fe<sub>3</sub>O<sub>4</sub>@CS@AF@Cu (Fig. 2, e) decreases its weight loss compared to Fe<sub>3</sub>O<sub>4</sub>@CS@AF (Fig. 2, d) is due to the generation of Cu(II) Schiff base complex, which results in the increase of inorganic component ratio of the composite materials. The amount of copper content (8.5%) into the catalyst

Fe<sub>3</sub>O<sub>4</sub>@CS@AF@Cu semi-quantitatively estimated from the difference between the mass loss of Fe<sub>3</sub>O<sub>4</sub>@CS@AF (Fig. 2, d) and Fe<sub>3</sub>O<sub>4</sub>@CS@AF@Cu (Fig. 2, e), respectively. The TGA estimation of copper content is in a good agreement with the ICP-OES analysis result of copper content of 8.01%. As there is no significant mass loss has been observed at a temperature of 575 °C and above, all of the composite materials exhibit remarkable stability.

The surface structure of the catalyst materials Fe<sub>3</sub>O<sub>4</sub>@CS@AF@Cu is studied using field-emission scanning electron microscopy (FE-SEM). Fig. 3 (a and b) represents the FE-SEM images of Fe<sub>3</sub>O<sub>4</sub>@CS@AF@Cu that have been captured at various magnifications and locations on the sample before the use of in the amination of aryl halide. The energy dispersive X-ray (EDX) mapping and elemental composition spectrum of the Fe<sub>3</sub>O<sub>4</sub>@CS@AF@Cu are also studied during the record of FE-SEM images. Fig. 3 (c and d) exhibits the elemental mapping and EDX spectrum of the catalyst material. The elemental composition and EDX spectra clearly prove that the magnetic Fe<sub>3</sub>O<sub>4</sub> core is successfully coated with chitosan. Then, the surface of the materials is functionalized by grafting furan-imine Schiff base, followed by the formation of a Cu(II) Schiff base complex on the same surface. Furthermore, it has been revealed that copper is evenly dispersed on the surface of the Fe<sub>3</sub>O<sub>4</sub>@CS@AF@Cu catalyst.

The morphology, size, and crystallinity of the Fe<sub>3</sub>O<sub>4</sub>@CS@AF@Cu are studied by transmission electron microscopy (TEM). Fig. 4 (a) shows TEM micrograph of Fe<sub>3</sub>O<sub>4</sub>@CS@AF@Cu is embedded into the CS matrix and coated onto the amorphous-carbon (a-c) film. The corresponding SAED pattern of the sample shows (Fig. 4; b) the diffraction peaks corresponding to the Fe<sub>3</sub>O<sub>4</sub>, and Cu which are consistent with the XRD analysis. Two sets of SAED rings are

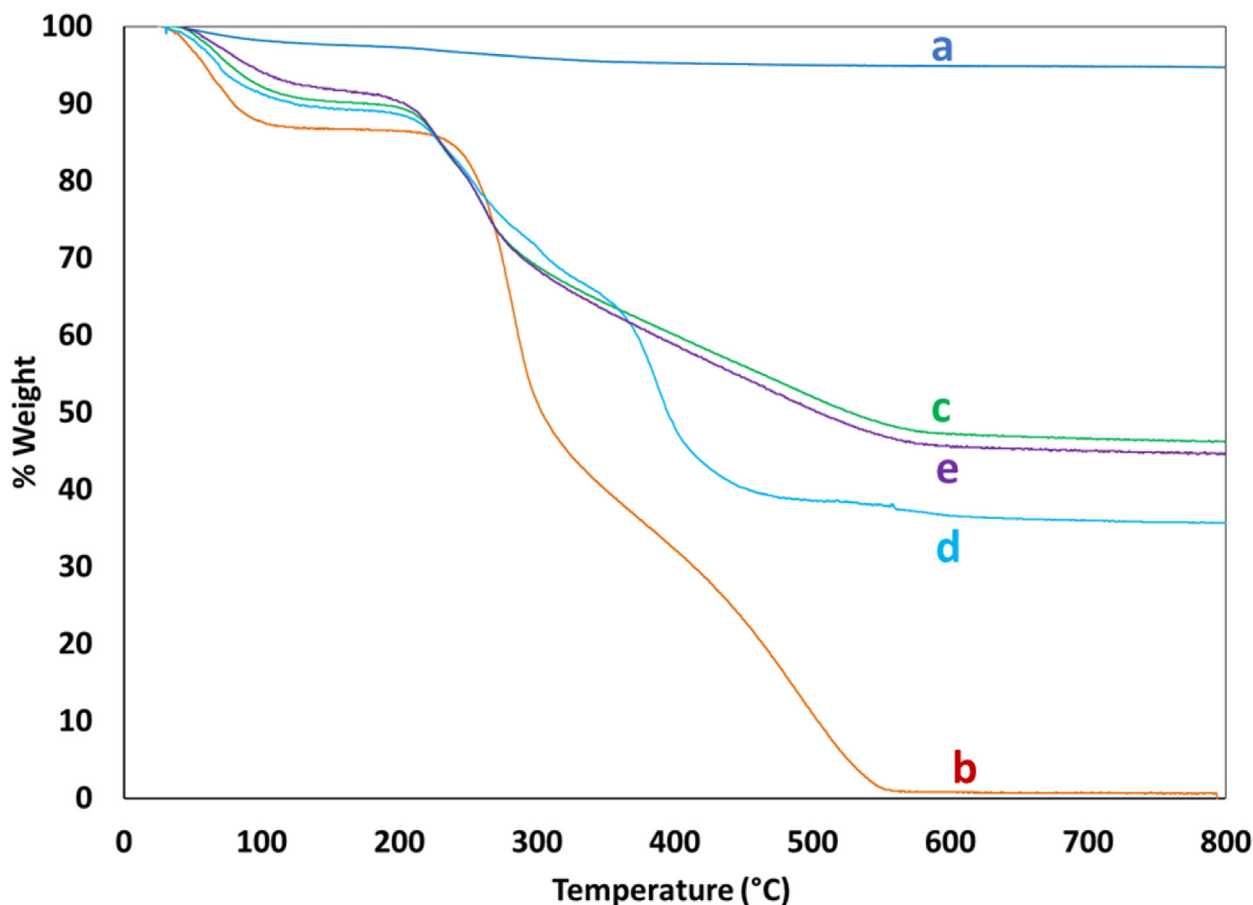


Fig. 2. TGA plots for Fe<sub>3</sub>O<sub>4</sub> (a), CS (b), Fe<sub>3</sub>O<sub>4</sub>@CS (c), Fe<sub>3</sub>O<sub>4</sub>@CS@AF (d), and Fe<sub>3</sub>O<sub>4</sub>@CS@AF@Cu (e).

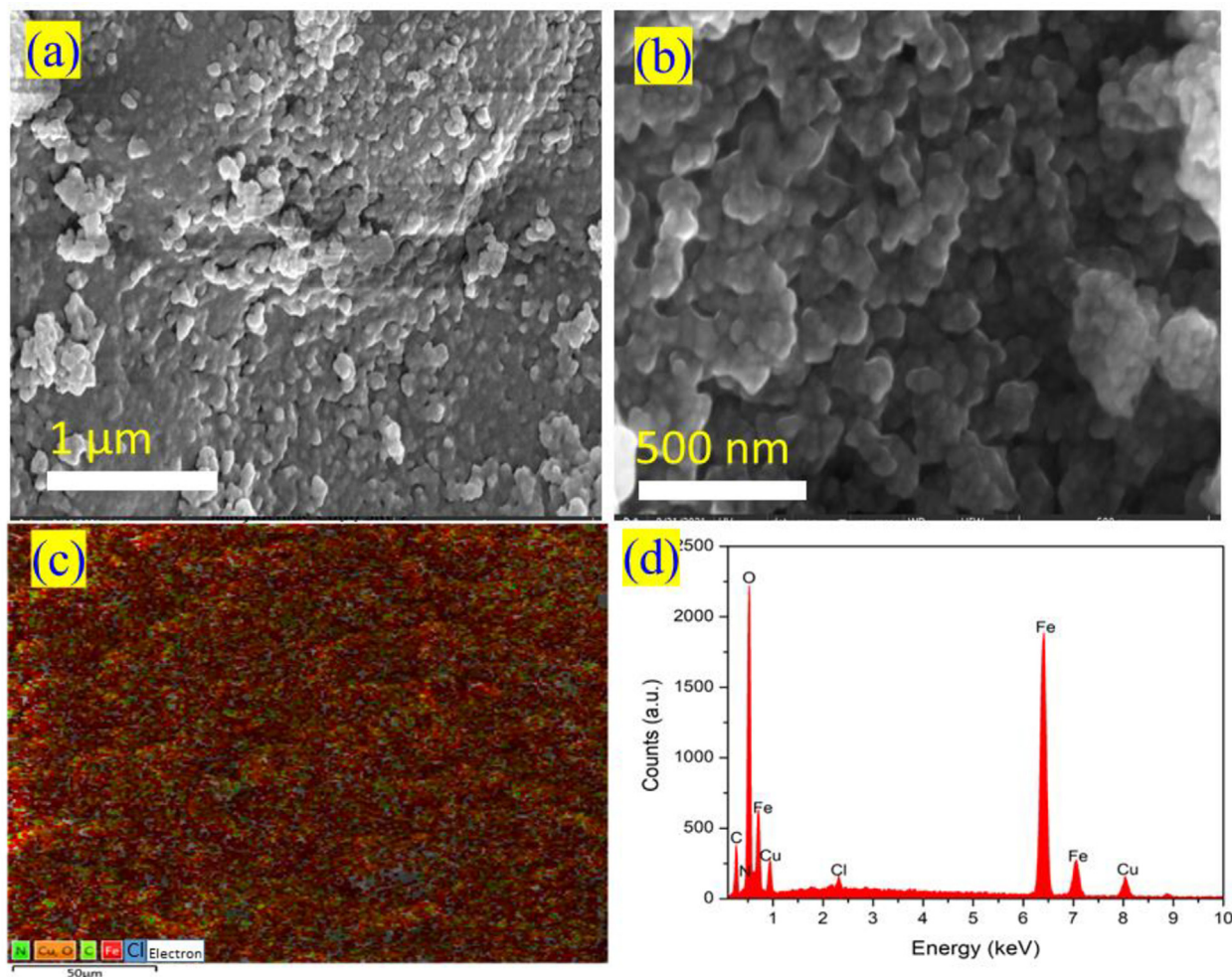


Fig. 3. FE-SEM images of  $\text{Fe}_3\text{O}_4\text{@CS@AF@Cu}$  (a) and (b) at different magnification, Energy dispersive X-ray (EDX) mapping (c) and elemental spectrum (d).

identified and indexed; 1st set corresponds to (111), (220), and (311), of fcc  $\text{Fe}_3\text{O}_4$  (JCPDS File no. 19-0629) (Prilepskii et al., 2018), while the 2nd set corresponds to (110), (221) and (241) of fcc  $\text{Cu(II)Cl}_2$  (JCPDS File no. 33-0451) (Han et al., 2003). An interplanar spacing of 0.29 nm corresponding to the (220) plane of  $\text{Fe}_3\text{O}_4$  is also identified (Fig. 4; c). An interplanar spacing of 3.09 Å corresponding to the (111) plane of  $\text{Cu(II)Cl}_2$  is also identified (Fig. 4; d). The HRTEM observation with SAED analysis shows the topotactic growth of  $\text{Cu(II)Cl}_2$  near the  $\text{Fe}_3\text{O}_4\text{@CS}$  matrix. The TEM image of  $\text{Fe}_3\text{O}_4\text{@CS@AF@Cu}$  after the 5th catalytic cycle is provided in SI Figure S3. The corresponding SAED pattern shows the diffraction peaks corresponding to the  $\text{Fe}_3\text{O}_4$ , and  $\text{Cu(II)Cl}_2$  which are consistent with the synthesised particles. No major structural and morphological changes in the  $\text{Fe}_3\text{O}_4\text{@CS@AF@Cu}$  after the 5th cycle of the catalytic reactions are observed (Figure S3).

XRD analysis is used for the determination of the crystallinity of the catalyst  $\text{Fe}_3\text{O}_4\text{@CS@AF@Cu}$ . XRD patterns of (a) bare  $\text{Fe}_3\text{O}_4$ , surface functionalized magnetic chitosan (b)  $\text{Fe}_3\text{O}_4\text{@CS@AF}$ , and the furan-imine Schiff base grafted  $\text{Cu(II)}$  complex (c)  $\text{Fe}_3\text{O}_4\text{@CS@AF@Cu}$  are represented in Fig. 5 for the comparison. All the composite materials (Fig. 5, a-c) exhibit peaks at  $2\theta = 30.2, 35.4, 43.2, 53.1, 57.2,$  and  $62.7$  corresponding to the reflections of (220), (311), (400), (422), (511), and (440) respectively. The appearance of these peaks proves that the crystalline core structure of  $\text{Fe}_3\text{O}_4$  remains intact in all composites, even after coating with CS and grafting of Schiff base. Furthermore, it is confirmed

that no phase transition occurs during this process, and the functionalization of  $\text{Fe}_3\text{O}_4$ 's surface with  $\text{Cu(II)}$  Schiff base complex. A similar behaviour for the  $\text{Fe}_3\text{O}_4$ -based functionalized materials has been previously reported (Zhang et al., 2010, Safari and Javadian 2014), and also been proven by the JCPDS card NO 75-1609 (Deng et al., 2005). The XRD pattern of  $\text{Fe}_3\text{O}_4\text{@CS@AF@Cu}$  also shows five additional peaks at  $2\theta = 21.9, 26.6, 28.8, 33.9, 35.4, 40.8$  and  $57.3^\circ$ , attributing to the reflection of (020), (101), (111), (201), (130), (221), and (241) respectively. The presence of these diffracted peaks confirms evidence that  $\text{Cu(II)}$  ions have been successfully coordinated onto the functionalized surface of magnetic chitosan (Han et al., 2003).

The surface chemical nature and chemical potential of metals that are present in  $\text{Fe}_3\text{O}_4\text{@CS@AF@Cu}$  are determined by XPS analysis. Fig. 6 (a) shows a wide range XPS curve of the catalyst material that exhibits the anticipated elements such C, N, O, Fe and Cu respectively. The narrow range XPS curve of carbon in the C 1s region shows peaks corresponds to the C-C, C-N, and C-O at 285.2, 286.7 and 288.4 eV respectively. Such peaks indicate an effective coating of  $\text{Fe}_3\text{O}_4$  with CS matrix and the generation of a Schiff base on the functionalized surface of  $\text{Fe}_3\text{O}_4$ -chitosan.

The XPS curve of N 1s shows peaks corresponding to the C = N and  $\text{NH}_2$ -C bonds present in the Schiff base ligand and chitosan moiety onto  $\text{Fe}_3\text{O}_4\text{@CS@AF@Cu}$  composite. The XPS curve of O 1s shows peaks that correspond to the Fe-O and C-O bonds. The high-resolution Fe 2p scan exhibits two peaks corresponding to

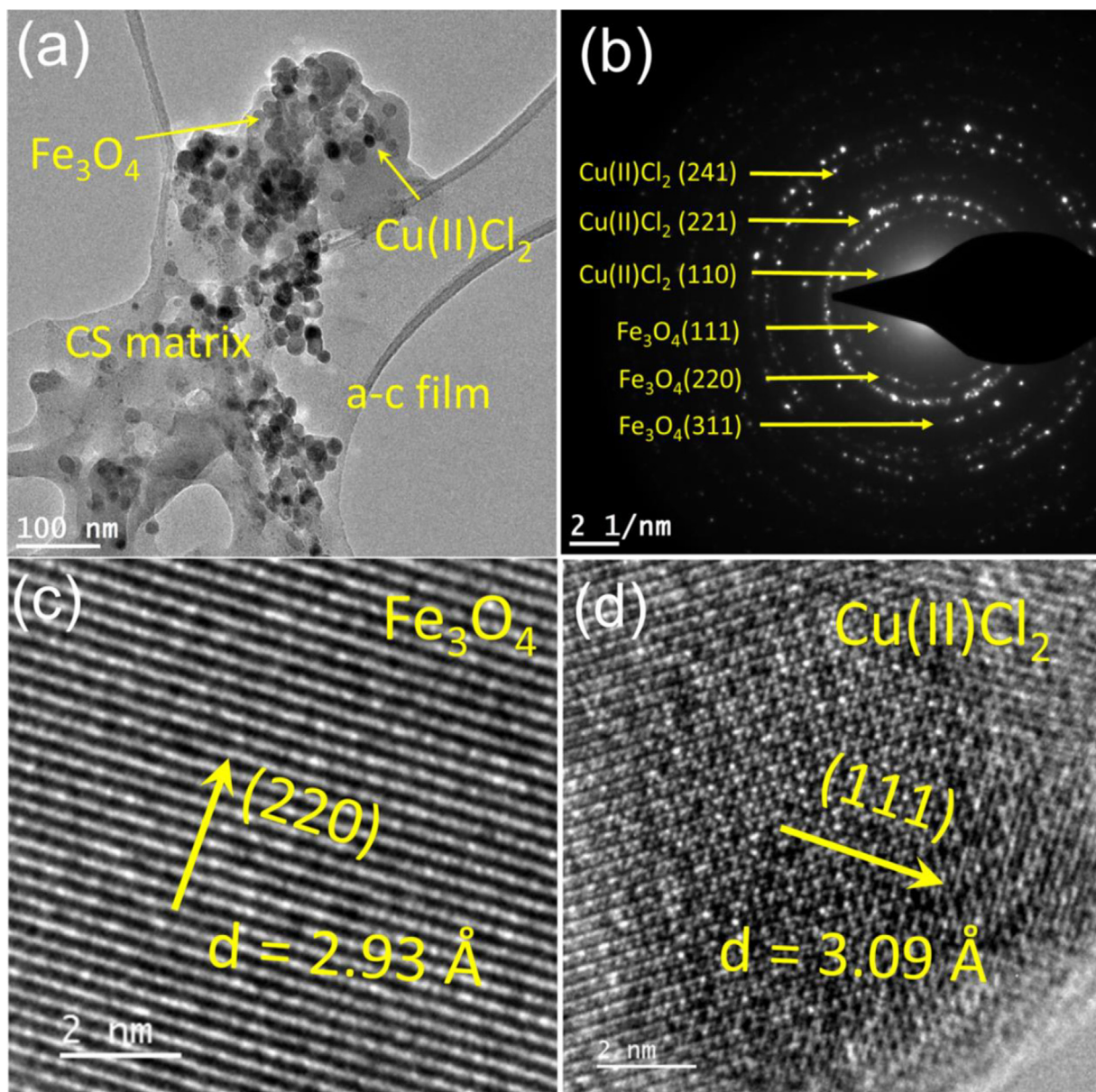


**Fig. 4.** (a) The TEM micrograph shows that  $\text{Fe}_3\text{O}_4@\text{CS}@\text{AF}@\text{Cu}$  is embedded into the CS matrix and coated onto the amorphous-carbon film. (b) The SAED pattern of the sample showing the  $\text{Fe}_3\text{O}_4$  and  $\text{Cu}(\text{II})\text{Cl}_2$  indices. (c) A high-resolution TEM micrograph of  $\text{Fe}_3\text{O}_4$  showing the interplanar spacing of 2.93 Å in the (220) growth direction. (d) A HRTEM micrograph showing  $\text{Cu}(\text{II})\text{Cl}_2$  showing interplanar spacing of 3.09 Å in the (111) growth direction.

$\text{Fe } 2p_{3/2}$  and  $\text{Fe } 2p_{1/2}$  at 711.0 and 722.3 eV, confirming the existence of  $\text{Fe}_3\text{O}_4$  core in the  $\text{Fe}_3\text{O}_4@\text{CS}@\text{AF}@\text{Cu}$ . Noticeably, these two peaks of  $\text{Fe}_3\text{O}_4$  appear in low intensity, due to the successful coating with CS, that is followed by the generation of Schiff base ligand. The XPS curve within the 930 to 970 eV range reveals peaks at 942.7 and 952.4 eV, which correspond to the binding energies of  $\text{Cu } 2p_{3/2}$  and  $\text{Cu } 2p_{1/2}$ , respectively.

This confirms the formation of a  $\text{Cu}(\text{II})$  Schiff base complex on the functionalized surface of  $\text{Fe}_3\text{O}_4$ -chitosan. Following successful characterization of  $\text{Fe}_3\text{O}_4@\text{CS}@\text{AF}@\text{Cu}$  catalyst material using various techniques such as FTIR, TGA, XRD FE-SEM, SEM-EDX, TEM, and XPS, the precise amount of copper content present on the catalyst has been estimated using ICP-OES analysis. The results from the analysis indicated that the copper loading in the  $\text{Fe}_3\text{O}_4@\text{CS}@\text{AF}@\text{Cu}$  catalyst material is 8.01% (w/w). **Section 4** of the [supporting information](#) provides the details on the experimental procedure for ICP-OES analysis to determine copper composition

in the catalyst material. Our findings indicate that Cu is efficiently deposited on the surface of the catalyst system via the generation of  $\text{Cu}(\text{II})$  Schiff base complex through the furan-imine coordination site, as is confirmed by all physicochemical characterization techniques employed.

### 3.2. Catalytic activity of $\text{Fe}_3\text{O}_4@\text{CS}@\text{AF}@\text{Cu}$ for the amination of aryl halides

Following the state-of-art characterisation, the catalytic activity of  $\text{Fe}_3\text{O}_4@\text{CS}@\text{AF}@\text{Cu}$  is investigated in the amination of aryl halides via the C-N bond formation reaction. Initially, 1-bromo-4-nitrobenzene and piperidine are chosen as standard substrates for the amination of aryl halides employing  $\text{Fe}_3\text{O}_4@\text{CS}@\text{AF}@\text{Cu}$  as catalyst (**Scheme 2**). The results for the optimization of the catalyst screening by varying the parameters such as catalyst loadings, base, temperature and reaction times for the C-N coupling reaction

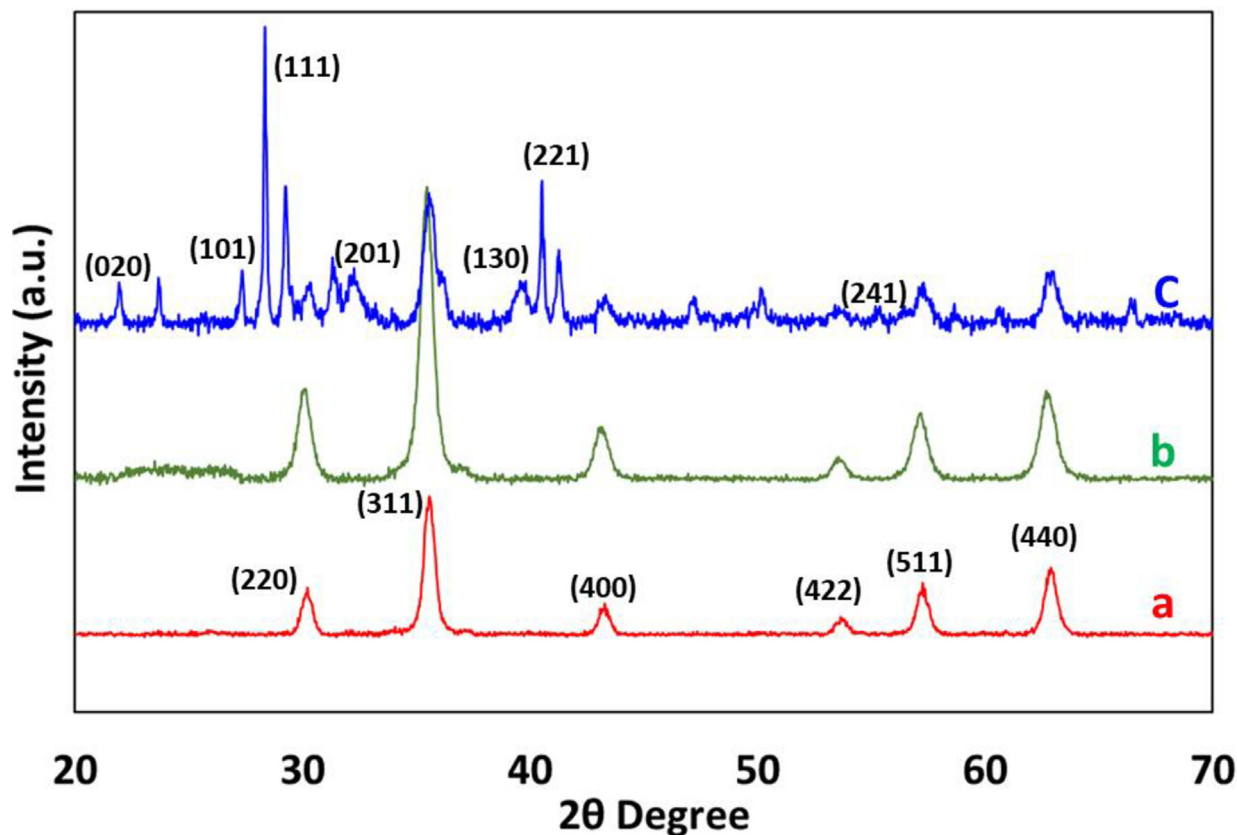


Fig. 5. XRD pattern of (a) bare  $\text{Fe}_3\text{O}_4$ , (b) surface functionalized magnetic chitosan  $\text{Fe}_3\text{O}_4@CS@AF$ , and (c) the furan-imine Schiff base grafted  $\text{Cu(II)}$  complex  $\text{Fe}_3\text{O}_4@CS@AF@Cu$ .

between 1-bromo-4-nitrobenzene and piperidine are summarized in Table S2 in the supporting information. The progress of the reaction is monitored by the thin layer chromatography (TLC), the conversion and product yield are estimated by gas chromatography-mass spectrometry (GCMS) and  $^1\text{H}$  NMR. Initially, the amination reaction is carried out in an aqueous medium in the absence of  $\text{Fe}_3\text{O}_4@CS@AF@Cu$ , to check the requirement of the catalyst for the target reaction. Noticeably, no detectable traces of the desired products are obtained after 16 h of reflux at  $100^\circ\text{C}$  in presence of 2.0 equivalent of base  $\text{K}_2\text{CO}_3$  (Table S2, entries 1–2). However, 10–15 % of the products are obtained in the presence of 20 mg of bare  $\text{Fe}_3\text{O}_4$  and surface functionalized  $\text{Fe}_3\text{O}_4@CS@AF$ .

(Table S2, entries 3–4) under the same reaction conditions. Remarkably, the product yield is increased to 85%, while 20 mg (2.5 mol% Cu)  $\text{Fe}_3\text{O}_4@CS@AF@Cu$  has been used in the same investigated conditions (Table S2, entry 5). For verifying the compatibility of the base, products yields are decreases to 80–65% when  $\text{KHCO}_3$  and  $\text{NaHCO}_3$  are used instead of  $\text{K}_2\text{CO}_3$  (Table S2, entries 6–7). For optimizing the heating condition, MW heating is introduced instead of traditional heating. 2 h MW heating in place of 16 h traditional heating at  $100^\circ\text{C}$ , product yield is increased from 85 to 95% (Table S2, entry 8). This is not surprising as MW heating is fast and more selective. Then, the amount of catalyst loadings is optimized by varying the catalyst amount from 20 to 2.5 mg. It is found that 5.0 mg of the catalyst produces the highest 98% of the desired products (Table S2, entries 9–11). Finally, the reaction time is optimized by changing from 2 h to 0.5 h and 1 h of MW heating produces the same 98% desired product (Table S2, entries 12–13).

After getting the optimized reaction conditions, the applicability of the  $\text{Fe}_3\text{O}_4@CS@AF@Cu$  catalyst is extended to other aryl halides and amines for the Ullmann C-N bond formation reactions.

Substrate scope of amination of different aryl halides with different amines using  $\text{Fe}_3\text{O}_4@CS@AF@Cu$  is summarized in the Table 1. 1-bromo-4-nitrobenzene produces 99% of the desired arylated amine 1-(4-nitrophenyl) piperidine with piperidine under 1 h MW heating at  $100^\circ\text{C}$  (Table S2, entry 3). At the optimized reaction conditions, 1-iodo-4-nitrobenzene also produces excellent yield of desired aryl amines with piperidine and pyrrolidine (Table 1, 3a and 3b). Similarly, a 98% of 1-(4-nitrophenyl)pyrrolidine product is obtained in the case of arylation between 1-bromo-4-nitrobenzene and pyrrolidine (Table 1, 3d). Aryl halides of fluoro, bromo, and iodo (F, Br and I) with CHO-substituents produce excellent yield (99–94 %) of desired Ullmann C-N coupled products (Table 1, 3e–3m) with high TON and TOF (Table S3, entries 5–13). Similarly, aryl halides of bromo and iodo (Br and I) with  $\text{COCH}_3$ -group, also produce the high yield of aminated products (Table S3, entries 14–18). The  $\text{Fe}_3\text{O}_4@CS@AF@Cu$  catalyst exhibits exceptional catalytic activity for the amination of various aryl halides with secondary amines, under energy-efficient microwave irradiation and in the environmentally friendly solvent water for facilitating Ullmann-type C-N bond formation reactions. Details substrate scope results including temperature, TON and TOF are summarized in Table S3 in the supporting information.

A comparison of the studied  $\text{Fe}_3\text{O}_4@CS@AF@Cu$  catalyst for the arylation of amines with previously reported  $\text{Fe}_3\text{O}_4$  based heterogeneous catalysts is presented in the Table S4 in the supporting information.

A hot gravity leaching experiment is carried out for the determination of the type of catalyst, either completely heterogeneous or homogeneous. Initially, the arylation of the amine reaction within 1-bromo-4-nitrobenzene and piperidine is quenched within 20 min from the beginning of the reaction under microwave irradiation.

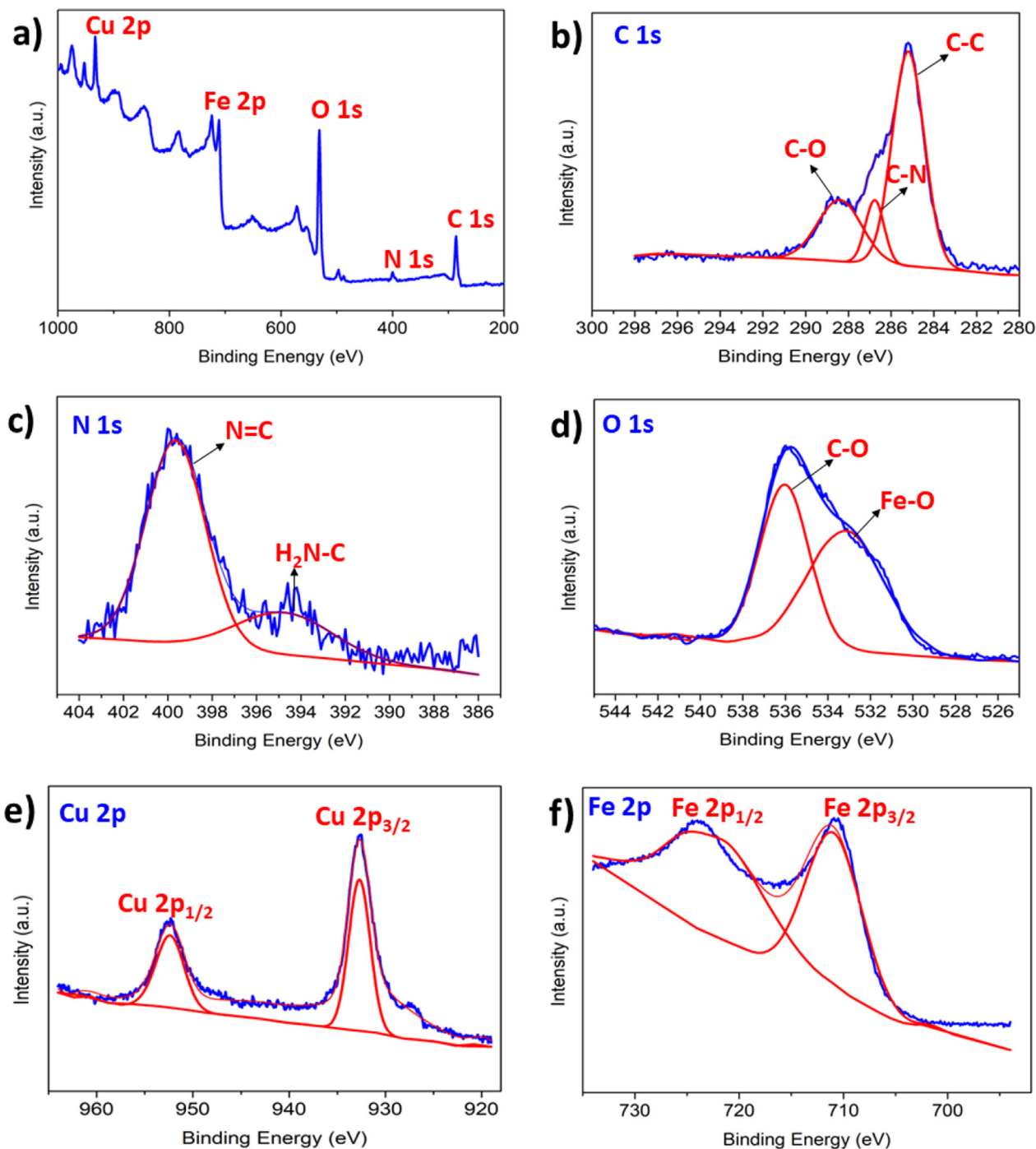
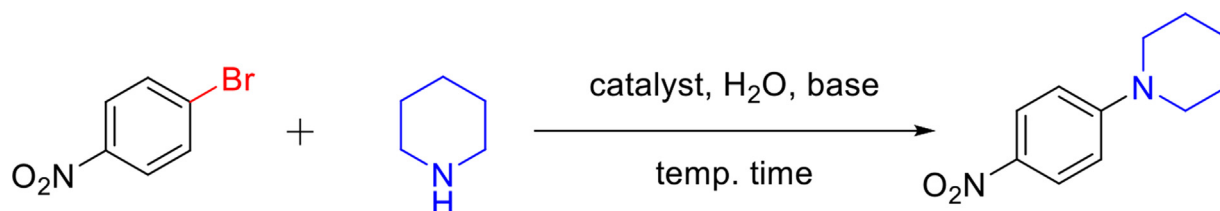
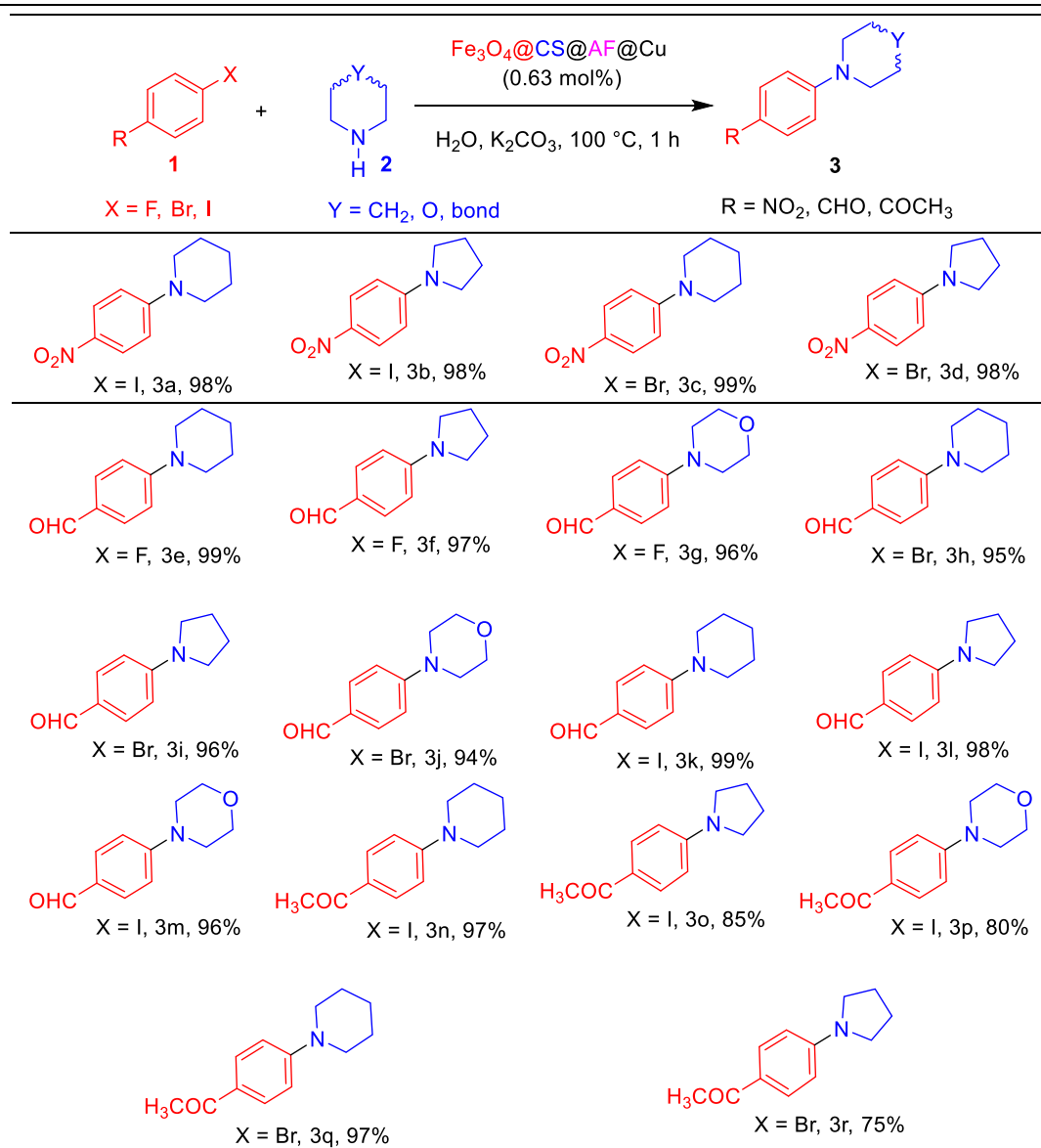


Fig. 6. XPS spectra of  $\text{Fe}_3\text{O}_4@\text{CS}@\text{AF}@\text{Cu}$ : a) full range, b) C 1s, c) N 1s, d) O 1s, e) Cu 2p, and f) Fe 2p.



Scheme 2. Amination of 1-bromo-4-nitrobenzene with piperidine. Reaction conditions: 1-bromo-4-nitrobenzene (1.0 mmol), piperidine (1.1 mmol), base (2.0 mmol), solvent  $\text{H}_2\text{O}$  (5 mL), catalyst  $\text{Fe}_3\text{O}_4@\text{CS}@\text{AF}@\text{Cu}$ .

**Table 1**Substrate scope of amination of different aryl halides with different amines using  $\text{Fe}_3\text{O}_4@\text{CS}@\text{AF}@\text{Cu}^a$ <sup>a</sup> Reaction conditions: aryl halide (1.0 mmol), amine (1.1 mmol),  $\text{K}_2\text{CO}_3$  (2.0 mmol),  $\text{H}_2\text{O}$  (5 mL), catalyst  $\text{Fe}_3\text{O}_4@\text{CS}@\text{AF}@\text{Cu}$  (5 mg, 0.63 mol% Cu).

ation (Fig. 7, a). Then, a hot gravity filtration is conducted for separating the solid catalyst from the reaction mixture and 30% of the desired product is detected by monitoring the filtrate of the reaction via GCMS (SI, section 8). Again, the filtrate of the reaction is continued for further 40 min under the same reaction conditions. The same product yield of 30% as is reported before (SI, section 8). This suggests that the active species responsible for the C-N coupling remains associated with the solid state and is not present in the solution phase. Therefore, these observations prove that the catalyst which is used in the arylation of amine reaction is indeed heterogeneous with no noticeable amount of Cu has leached during the course of the reaction. Furthermore, ICP-OES analysis of the used catalyst reveals copper content 7.90% which is close to the original 8.01%. In addition, other characterizations of the used

catalyst including FE-SEM (Figure S1), and TEM (Figure S3) show the same chemical and morphological properties as is stated before.

Easy and simple separation of the catalyst from the reaction mixture using an external magnet is the prime advantage of the  $\text{Fe}_3\text{O}_4$  based heterogeneous catalyst. This magnetic separation makes  $\text{Fe}_3\text{O}_4$ -based heterogeneous catalyst very attractive in industrial applications due to its ease of recycling and reusable capability. The recycling and reusability of the studied catalyst  $\text{Fe}_3\text{O}_4@\text{CS}@\text{AF}@\text{Cu}$  is investigated for the amination of 1-bromo-4-nitrobenzene with piperidine under optimized conditions (Fig. 7, b).

Upon completion of each cycle of the reaction, the catalyst  $\text{Fe}_3\text{O}_4@\text{CS}@\text{AF}@\text{Cu}$  is removed in presence of an external magnet and

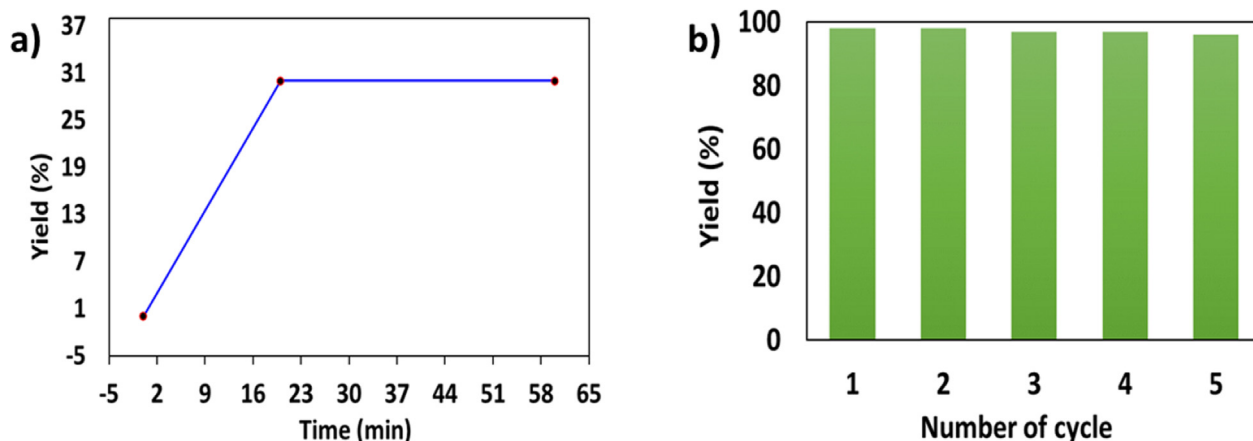


Fig. 7. (a) Hot gravity leaching experiment of the catalyst  $\text{Fe}_3\text{O}_4\text{CS@AF@Cu}$  for the arylation of 1-bromo-4-nitrobenzene and piperidine using under optimized conditions and (b) Reusing capacity of the catalyst  $\text{Fe}_3\text{O}_4\text{CS@AF@Cu}$  for the amination of 1-bromo-4-nitrobenzene with piperidine.

dried in vacuum after being washed three times with EtOH (3x 10 mL). The same catalyst has repeatedly been used for 5th cycles of the reaction and found no significant loss of catalytic activity.

#### 4. Conclusions

In summary, a novel heterogeneous  $\text{Fe}_3\text{O}_4$ -chitosan immobilized Cu(II) Schiff base catalyst  $\text{Fe}_3\text{O}_4\text{CS@AF@Cu}$  is successfully synthesized and well characterized with state-of-art techniques. The catalyst demonstrates an excellent catalytic activity for the Ullmann C-N coupling reactions for the amination of aryl halides. A variety of aryl halides (F, Br and I) with different substituents such as  $-\text{CHO}$ ,  $-\text{NO}_2$  and  $-\text{COCH}_3$  are applicable for the amination with secondary amines under the investigated conditions. Furthermore, the catalyst  $\text{Fe}_3\text{O}_4\text{CS@AF@Cu}$  is recovered with an external magnet from the reaction mixture and reused for five times without noticeable loss of its catalytic performance. Overall, the catalyst is fabricated using non-toxic and cheap metal (Fe and Cu) and with bio renewable feedstock chitosan. Therefore, this catalyst can be integrated in a practical and convenient C-N coupling reactions where a cost-effective and sustainable method is applicable.

#### Declaration of Competing Interest

The authors declare that they have no known competing financial interests or personal relationships that could have appeared to influence the work reported in this paper.

#### Appendix A. Supplementary material

Supplementary data to this article can be found online at <https://doi.org/10.1016/j.arabjc.2023.105317>.

#### References

- Ahmad, I., Shagufta, R.D., et al., 2021. An environmentally benign solid acid nanocatalyst for the green synthesis of carboxylic acid ester. *ChemistrySelect* 6, 9645–9652. <https://doi.org/10.1002/slct.202102230>.
- Aubin, Y., Fischmeister, C., Thomas, C.M., et al., 2010. Direct amination of aryl halides with ammonia. *Chem. Soc. Rev.* 39, 4130–4145.
- Baek, J., Rungtaweeworanit, B., Pei, X., et al., 2018. Bioinspired metal-organic framework catalysts for selective methane oxidation to methanol. *J. Am. Chem. Soc.* 140, 18208–18216. <https://doi.org/10.1021/jacs.8b11525>.
- Bromho, T.K., Ibrahim, K., Kabir, H., et al., 2018. Understanding the impacts of Al<sup>3+</sup>-substitutions on the enhancement of magnetic, dielectric and electrical behaviors of ceramic processed nickel-zinc mixed ferrites: FTIR assisted

- studies. *Mater. Res. Bull.* 97, 444–451. <https://doi.org/10.1016/j.materresbull.2017.09.013>.
- Cai, W., Guo, M., Weng, X., et al., 2019. Adsorption of doxorubicin hydrochloride on glutaric anhydride functionalized  $\text{Fe}_3\text{O}_4\text{@SiO}_2$  magnetic nanoparticles. *Mater. Sci. Eng. C* 98, 65–73. <https://doi.org/10.1016/j.msec.2018.12.145>.
- Chouhan, G., Wang, D., Alper, H., 2007. Magnetic nanoparticle-supported proline as a recyclable and recoverable ligand for the CuI catalyzed arylation of nitrogen nucleophiles. *Chem. Commun.* 4809–4811. <https://doi.org/10.1039/B711298J>.
- Deng, H., Li, X., Peng, Q., et al., 2005. Monodisperse magnetic single-crystal ferrite microspheres. *Angew. Chem. Int. Ed.* 44, 2782–2785. <https://doi.org/10.1002/anie.200462551>.
- Diab, M., El-Sonbati, A., Bader, D., et al., 2012. Thermal stability and degradation of chitosan modified by acetophenone. *J. Polym. Environ.* 20, 29–36.
- Dorel, R., Grugel, C.P., Haydl, A.M., 2019. The Buchwald-Hartwig amination after 25 years. *Angew. Chim. Int. Ed.* 58, 17118–17129. <https://doi.org/10.1002/anie.201904795>.
- Duan, L., Guo, S., Yang, J., et al., 2009. Ultrasonic-assisted condensation of chitosan with salicylaldehyde. *Chin. J. Oceanol. Limnol.* 27, 882.
- Ge, X., Sun, F., Liu, X., et al., 2018. Mechanistic aspects of copper (II)-catalyzed synthesis of sulfones from sulfinate salts and aryl halides under C-S coupling. *Mol. Catal.* 449, 72–78. <https://doi.org/10.1016/j.mcat.2017.12.016>.
- Ge, X., Zhang, S., Chen, X., et al., 2019. A designed bi-functional sugar-based surfactant: micellar catalysis for C-X coupling reaction in water. *Green Chem.* 21, 2771–2776. <https://doi.org/10.1039/C9GC00964G>.
- Gómez-Orellana, P., Lledós, A., Ujaque, G., 2021. Computational analysis on the Pd-catalyzed C-N coupling of ammonia with aryl bromides using a chelate phosphine ligand. *J. Org. Chem.* 86, 4007–4017. <https://doi.org/10.1021/acs.joc.0c02865>.
- Han, M.S., Lee, B.G., Ahn, B.S., et al., 2003. Surface properties of CuCl<sub>2</sub>/AC catalysts with various Cu contents: XRD, SEM, TG/DSC and CO-TPD analyses. *Appl. Surf. Sci.* 211, 76–81. [https://doi.org/10.1016/S0169-4332\(03\)00177-6](https://doi.org/10.1016/S0169-4332(03)00177-6).
- Hartwig, J.F., Kawatsura, M., Hauck, S.L., et al., 1999. Room-temperature palladium-catalyzed amination of aryl bromides and chlorides and extended scope of aromatic C-N bond formation with a commercial ligand. *J. Org. Chem.* 64, 5575–5580. <https://doi.org/10.1021/jo9904081>.
- Hasan, K., 2020. Methyl salicylate functionalized magnetic chitosan immobilized palladium nanoparticles: An efficient catalyst for the Suzuki and Heck coupling reactions in water. *ChemistrySelect* 5, 7129–7140. <https://doi.org/10.1002/slct.202001933>.
- Hasan, K., R. G. Joseph and S. P. Patole, 2022. Copper Pyrrole-imine Incorporated  $\text{Fe}_3\text{O}_4$ -Nanocomposite: A Magnetically Separable and Reusable Catalyst for the Oxidative Amination of Aryl Aldehydes. *ChemistrySelect*. 7, e202201840. <https://doi.org/https://doi.org/10.1002/slct.202201840>.
- Hasan, K., Shehadi, I.A., Al-Bab, N.D., et al., 2019. Magnetic chitosan-supported silver nanoparticles: A heterogeneous catalyst for the reduction of 4-nitrophenol. *Catalysts* 9. <https://doi.org/10.3390/catal9100839>.
- Hasan, K., Shehadi, I.A., Ahmed Bagudu, K., et al., 2022. Magnetic silica surface functionalized palladium catalyst: A modular approach for C-C cross-coupling reactions in water. *Appl. Surf. Sci.* 571. <https://doi.org/10.1016/j.apsusc.2021.151369>.
- Hasan, K., Joseph, R.G., Patole, S.P., et al., 2023. Development of magnetic  $\text{Fe}_3\text{O}_4$ -chitosan immobilized Cu(II) Schiff base catalyst: An efficient and reusable catalyst for microwave assisted one-pot synthesis of propargylamines via A3 coupling. *Catal. Commun.* 174. <https://doi.org/10.1016/j.catcom.2022.106588>.
- Hasan, K., Zysman-Colman, E., 2013. The effect of aryl substitution on the properties of a series of highly absorptive Cationic Iridium(III) complexes bearing ancillary bis(arylimino)acenaphthene ligands. *Eur. J. Inorg. Chem.* 2013, 4421–4429. <https://doi.org/10.1002/ejic.201300583>.

- Hazari, N., Melvin, P.R., Beromi, M.M., 2017. Well-defined nickel and palladium precatalysts for cross-coupling. *Nat. Rev. Chem.* 1. <https://doi.org/10.1038/s41570-017-0025>.
- Iftime, M.-M., S. Morariu and L. J. C. p. Marin, 2017. Salicyl-imine-chitosan hydrogels: Supramolecular architecturing as a crosslinking method toward multifunctional hydrogels. *Carbohydrate Polymers*. 165, 39–50.
- Islam, S.M., Mondal, S., Mondal, P., et al., 2012. A reusable polymer supported copper catalyst for the C-N and C-O bond cross-coupling reaction of aryl halides as well as arylboronic acids. *J. Organomet. Chem.* 696, 4264–4274. <https://doi.org/10.1016/j.jorganchem.2011.10.004>.
- Jayakumar, R., Nwe, N., Tokura, S., et al., 2007. Sulfated chitin and chitosan as novel biomaterials. *Int. J. Biol. Macromol.* 40, 175–181.
- Khaleel, A., I. Shehadi and M. J. J. o. n.-c. s. Al-Shamisi, 2010. Structural and textural characterization of sol-gel prepared nanoscale titanium-chromium mixed oxides. *Journal of Non-Crystalline Solids*. 356, 1282–1287.
- Khaleel, A., I. Shehadi and A. J. F. p. t. Al-Marzouqi, 2011. Catalytic conversion of chloromethane to methanol and dimethyl ether over mesoporous  $\gamma$ -alumina. *Fuel Processing Technology*. 92, 1783–1789.
- Kim, H.-R., J.-W. Jang and J.-W. J. J. o. h. m. Park, 2016. Carboxymethyl chitosan-modified magnetic-cored dendrimer as an amphoteric adsorbent. *Journal of Hazardous Materials*. 317, 608–616.
- Lang, F., Zewge, D., Houpis, I.N., et al., 2001. Amination of aryl halides using copper catalysis. *Tetrahedron Lett.* 42, 3251–3254. [https://doi.org/10.1016/S0040-4039\(01\)00458-0](https://doi.org/10.1016/S0040-4039(01)00458-0).
- Lei, Z., Pang, X., Li, N., et al., 2009. A novel two-step modifying process for preparation of chitosan-coated Fe<sub>3</sub>O<sub>4</sub>/SiO<sub>2</sub> microspheres. *J. Mater. Process. Technol.* 209, 3218–3225.
- Liu, X., Chang, S., Chen, X., et al., 2018. Efficient Ullmann C-X coupling reaction catalyzed by a recoverable functionalized-chitosan supported copper complex. *New J. Chem.* 42, 16013–16020. <https://doi.org/10.1039/C8NJ02677G>.
- Liu, Z., Wang, H., Li, B., et al., 2012. Biocompatible magnetic cellulose-chitosan hybrid gel microspheres reconstituted from ionic liquids for enzyme immobilization. *J. Mater. Chem.* 22, 15085–15091.
- Lo, Q.A., Sale, D., Braddock, D.C., et al., 2018. Mechanistic and Performance Studies on the Ligand-Promoted Ullmann Amination Reaction. *ACS Catal.* 8, 101–109. <https://doi.org/10.1021/acscatal.7b03664>.
- Mohammadikish, M. and S. H. J. J. o. M. S. Hashemi, 2019. Functionalization of magnetite-chitosan nanocomposite with molybdenum complexes: new efficient catalysts for epoxidation of olefins. *Journal of Materials Science*. 54, 6164–6173.
- Monier, M., Ayad, D.M., Wei, Y., et al., 2010. Adsorption of Cu(II), Co(II), and Ni(II) ions by modified magnetic chitosan chelating resin. *J. Hazard. Mater.* 177, 962–970. <https://doi.org/10.1016/j.jhazmat.2010.01.012>.
- Moradi, M., Elahinia, A., Vasseghian, Y., et al., 2020. A review on pollutants removal by Sono-photo-Fenton processes. *J. Environ. Chem. Eng.* 8, 104330.
- Moulijn, J.A., van Leeuwen, P.W., van Santen, R.A., 1993. Catalysis: an integrated approach to homogeneous, heterogeneous and industrial catalysis. Elsevier.
- Panda, N., Jena, A.K., Mohapatra, S., et al., 2011. Copper ferrite nanoparticle-mediated N-arylation of heterocycles: a ligand-free reaction. *Tetrahedron Lett.* 52, 1924–1927. <https://doi.org/10.1016/j.tetlet.2011.02.050>.
- Panigrahi, S., Basu, S., Praharaj, S., et al., 2007. Synthesis and size-selective catalysis by supported gold nanoparticles: study on heterogeneous and homogeneous catalytic process. *J. Phys. Chem. C* 111, 4596–4605.
- Pelletier, J.D.A., Basset, J.-M., 2016. Catalysis by design: Well-defined single-site heterogeneous catalysts. *Acc. Chem. Res.* 49, 664–677. <https://doi.org/10.1021/acs.accounts.5b00518>.
- Poshina, D.N., Raik, S.V., Poshin, A.N., et al., 2018. Accessibility of chitin and chitosan in enzymatic hydrolysis: A review. *Polym. Degrad. Stab.* 156, 269–278.
- Prilepskii, A., Fakhardo, A., Drozdov, A., et al., 2018. Urokinase-conjugated magnetite nanoparticles as a promising drug delivery system for targeted thrombolysis: Synthesis and preclinical evaluation. *ACS Appl. Mater. Interfaces* 10. <https://doi.org/10.1021/acsami.8b14790>.
- Raiza, A.J., Pandian, K., Kumar, R.G., 2019. Biosynthesis of copper nanoparticles supported on zeolite Y and its application in catalytic C-N cross coupling reactions between amines and aryl halides. *ChemistrySelect* 4, 1964–1970. <https://doi.org/10.1002/slct.201804003>.
- Rana, M.S., Halim, M.A., Hoque, S.A.M.W., et al., 2009. Bioadsorption of arsenic by prepared and commercial crab shell chitosan. *Biotechnology* 8, 160–165. <https://doi.org/10.3923/biotech.2009.160.165>.
- Reddy, P.L., Arundhathi, R., Rawat, D.S., 2015. Cu(0)/Al<sub>2</sub>O<sub>3</sub>/SiO<sub>2</sub> NPs: an efficient reusable catalyst for the cross coupling reactions of aryl chlorides with amines and anilines. *RSC Adv.* 5, 92121–92127. <https://doi.org/10.1039/C5RA19337K>.
- Safari, J., Javadian, L., 2014. Chitosan decorated Fe<sub>3</sub>O<sub>4</sub> nanoparticles as a magnetic catalyst in the synthesis of phenytoin derivatives. *RSC Adv.* 4, 48973–48979. <https://doi.org/10.1039/C4RA06618A>.
- Sashiwa, H., Kawasaki, N., Nakayama, A., et al., 2002. Chemical modification of chitosan. 14: Synthesis of water-soluble chitosan derivatives by simple acetylation. *Biomacromolecules* 3, 1126–1128. <https://doi.org/10.1021/bm0200480>.
- Shahraki, S., H. S. Delarami and F. J. I. j. o. b. m. Khosravi, 2019. Synthesis and characterization of an adsorptive Schiff base-chitosan nanocomposite for removal of Pb (II) ion from aqueous media. *International journal of biological macromolecules*. 139, 577–586.
- Sharma, R., Y. Monga and A. J. J. o. M. C. A. C. Puri, 2014. Magnetically separable silica@Fe<sub>3</sub>O<sub>4</sub> core-shell supported nano-structured copper (II) composites as a versatile catalyst for the reduction of nitroarenes in aqueous medium at room temperature. *Journal of Molecular Catalysis A: Chemical*. 393, 84–95.
- Sun, X., Shen, J., Yu, D., et al., 2019. Preparation of pH-sensitive Fe<sub>3</sub>O<sub>4</sub>@C/carboxymethyl cellulose/chitosan composite beads for diclofenac sodium delivery. *Int. J. Biol. Macromol.* 127, 594–605.
- Tajyani, S. and A. J. J. o. E. C. Babaei, 2018. A new sensing platform based on magnetic Fe<sub>3</sub>O<sub>4</sub>@NiO core/shell nanoparticles modified carbon paste electrode for simultaneous voltammetric determination of Quercetin and Tryptophan. *Journal of Electroanalytical Chemistry*. 808, 50–58.
- Terrasson, V. and E. Guenin, 2018. Nanomagnetic-Supported Catalysts. *Novel Magnetic Nanostructures*, Elsevier: 333–371.
- Ulu, A., Birhanli, E., Boran, F., et al., 2020. Laccase-conjugated thiolated chitosan-Fe<sub>3</sub>O<sub>4</sub> hybrid composite for biocatalytic degradation of organic dyes. *Int. J. Biol. Macromol.* 150, 871–884.
- Wagaw, S., Buchwald, S.L., 1996. The synthesis of aminopyridines: A method employing palladium-catalyzed carbon-nitrogen bond formation. *J. Org. Chem.* 61, 7240–7241. <https://doi.org/10.1021/jo9612739>.
- Wu, D., Wang, Y., Li, Y., et al., 2019. Phosphorylated chitosan/CoFe<sub>2</sub>O<sub>4</sub> composite for the efficient removal of Pb(II) and Cd(II) from aqueous solution: Adsorption performance and mechanism studies. *J. Mol. Liq.* 277, 181–188. <https://doi.org/10.1016/j.molliq.2018.12.098>.
- Xie, W., Han, Y., Wang, H., 2018. Magnetic Fe<sub>3</sub>O<sub>4</sub>/MCM-41 composite-supported sodium silicate as heterogeneous catalysts for biodiesel production. *Renew. Energy* 125, 675–681. <https://doi.org/10.1016/j.renene.2018.03.010>.
- Xu, X., X.-k. Ouyang and L.-Y. J. J. o. M. L. Yang, 2021. Adsorption of Pb (II) from aqueous solutions using crosslinked carboxylated chitosan/carboxylated nanocellulose hydrogel beads. *Journal of Molecular Liquids*. 322, 114523.
- Yadav, S., Jain, A., Malhotra, P., 2019. A review on the sustainable routes for the synthesis and applications of cuprous oxide nanoparticles and their nanocomposites. *Green Chem.* 21, 937–955. <https://doi.org/10.1039/C8GC03303J>.
- Yi, Z., Huang, M., Wan, Y., et al., 2018. An effective heterogeneous copper catalyst system for C-N coupling and its application in the preparation of 2-methyl-4-methoxydiphenylamine (MMDPA). *Synthesis (Germany)* 50, 3911–3920. <https://doi.org/10.1055/s-0037-1609578>.
- Zhang, Y., César, V., Storch, G., et al., 2014. Skeleton decoration of NHCs by amino groups and its sequential booster effect on the palladium-catalyzed Buchwald-Hartwig amination. *Angew. Chim. Int. Ed.* 53, 6482–6486. <https://doi.org/10.1002/anie.201402301>.
- Zhang, P., Yuan, J., Li, H., et al., 2013. Mesoporous nitrogen-doped carbon for copper-mediated Ullmann-type C-O/N-S cross-coupling reactions. *RSC Adv.* 3, 1890–1895. <https://doi.org/10.1039/c2ra22559j>.
- Zhang, Y., Zhang, J., Tian, M., et al., 2016. Fabrication of amino-functionalized Fe<sub>3</sub>O<sub>4</sub>@Cu<sub>3</sub>(BTC) 2 for heterogeneous Knoevenagel condensation. *Chin. J. Catal.* 37, 420–427.
- Zhang, L.-Y., Zhu, X.-J., Sun, H.-W., et al., 2010. Control synthesis of magnetic Fe<sub>3</sub>O<sub>4</sub>-chitosan nanoparticles under UV irradiation in aqueous system. *Curr. Appl Phys.* 10, 828–833. <https://doi.org/10.1016/j.cap.2009.10.002>.